Heliyon 6 (2020) e03763

Contents lists available at ScienceDirect

Heliyon

journal homepage: www.cell.com/heliyon

Research article

Ferromagnetic $FeSe_2$ from a mixed sulphur-selenium complex of iron [Fe{$(SePPh_2NPPh_2S)_2N$}$_3$] through pyrolysis

Temidayo Oyetunde [a,b,**], Martins O. Omorogie [a,c,*], Paul O'Brien [b,1]

[a] Centre for Chemical and Biochemical Research (CCBR), Department of Chemical Sciences, Redeemer's University, Ede, P.M.B. 230, Osun State, 232102, Nigeria
[b] School of Chemistry and School of Materials, The University of Manchester, Oxford Road, Manchester, M13 9PL, UK
[c] Water Science and Technology Research Unit, African Centre of Excellence for Water and Environmental Research (ACEWATER), Redeemer's University, Ede, P.M.B. 230, Osun State, 232102, Nigeria

ARTICLE INFO

Keywords:
Inorganic chemistry
Iron (III) thioselenoimidodiphosphinate
Ferromagnetic
$FeSe_2$
Single-source precursor
Iron chalcogenides

ABSTRACT

Iron (III) thioselenoimidodiphosphinate complex, Fe{$(SePPh_2NPPh_2S)_2N$}$_3$], was synthesized from the ligand [$Ph_2P(S)HNP(Se)Ph_2$], and the complex employed as the combined source of the targeted elements (Fe and Se) to generate orthorhombic $FeSe_2$. This was achieved by thermolysis using a quartz glass tube, under reduced pressure at 500 °C during 1 h 30 min. The crystalline product was revealed by X-ray diffraction (XRD), while the morphology consisted of polygonal crystallites according to the scanning electron microscopy (SEM) studies. Superconducting quantum interference device (SQUID) measurements on the material confirmed its ferromagnetism as observed from the magnetization curve, indicated by the field-cooled and zero field-cooled conditions under a magnetic field of 100 Oe. This ferromagnetic material, $FeSe_2$ finds useful application in producing electrical semiconductors.

1. Introduction

Iron chalcogenides have been widely investigated for diverse range of applications for example, hydrogen evolution, light energy conversion devices, batteries, extremely hot superconductors, high capacitance capacitors and storage devices [1, 2, 3, 4, 5, 6, 7]. In terms of usefulness, iron chalcogenides have been mostly studied as photovoltaics or supercapacitors, together with their magnetic properties. In a photovoltaic device, iron chalcogenides can behave as a photo-absorber layer [8]. The controllable properties of iron chalcogenides has resulted in their diverse applications. Some of these properties are: optics, electric, conductivity and magnetism [9, 10, 11, 12, 13]. The limited band-gap and large absorption coefficient make iron selenide a more important chalcogenide, with potential application in solar cells [12, 13, 14, 15, 16]. Other factors responsible for the high importance of iron selenide include magnetism, light-absorption and semiconducting features [17, 18, 19]. Iron selenide exists in three different types: tetragonal FeSe, NiAs-type phase (containing hexagonal Fe_7Se_8 and monoclinic Fe_3Se_4) and orthorhombic marcasite $FeSe_2$ [8,17,19].

Iron selenide thin films have been prepared through chemical vapour deposition (CVD) [19, 20, 21], electrolytic bath deposition [22] and pulsed laser deposition [23]. Clean FeSe films were produced from the reaction between iron pentacarbonyl and hydrogen selenide, but these precursors were extremely hazardous [19]. Akhtar *et al* [10] deposited FeSe thin films from iron (III) selenoureato precursor at 625 °C. A solution of iron selenourea complex in toluene using aerosol-assisted CVD (AACVD) produced complicated mixture of different phases [20].

The complex iron(II) bis(tetraisopropyldiselenoimidodiphosphinate) [Fe{$(SeP^iPr_2)_2N$}$_2$] served as a combined source of Fe and Se in a chemical vapour deposition supported by a catalyst and deposited FeSe and Fe_3Se_4 [21]. Mostly, the hot-injection technique has been used widely to prepare nanoparticles of iron selenide [8]. The complex ([Fe{$(SePR_2)_2N$}$_2$], R = ^{i}Pr or Ph) was decomposed in oleylamine and produced plate-like $FeSe_2$ crystallites [12]. Through a mixed precursor system, the reaction between iron (III) acetylacetonate and selenium in oleylamine generated nanocacti. However, this morphology was changed by the addition of oleic acid [24]. Nanoflakes of iron selenide were produced in a reaction in a reaction involving OAmine, OAcid, TOPSe and $FeCl_2$ [25]. The reaction between $FeCl_3$ and

* Corresponding author.
** Corresponding author.
E-mail addresses: oyetundetemi@run.edu.ng (T. Oyetunde), omorogiem@run.edu.ng, dromorogiemoon@gmail.com (M.O. Omorogie).
[1] Deceased.

https://doi.org/10.1016/j.heliyon.2020.e03763
Received 26 December 2019; Received in revised form 21 February 2020; Accepted 6 April 2020

imido(tetradiphenyldiselenodiphosphinate) [$(SePPh_2)_2N$] involved reduction, which produced bis(tetraphenyldiselenoimidodiphosphinato) iron (II) complex [12] rather than the tris compound. It is noteworthy to mention that the report on [$Fe\{(SePPh_2)_2N\}_2$] did not give any XRD analysis on the deposited $FeSe_2$. Also, there were no magnetic measurements reported on the material. However, in this present work, no reduction occurred between $FeCl_3$ and imido(tetradiphenylthioselenodiphosphanate) ligand [$Ph_2P(S)HNP(Se)Ph_2$], thereby producing the expected tris compound. As far as we know, it is not yet documented that a mixed dichalcogenoimidodiphosphinate complex of iron serves as a combined source of the targeted elements to synthesise iron diselenide.

Iron diselenide, $FeSe_2$ is a ferroselite material with an orthorhombic geometry, which is an important semiconductor with an appropriate band gap ($E_g = 1.0$ eV) [15] and coefficient of absorption (5×10^5 cm^{-1}) [26], making it applicable in light energy conversion and photoelectrochemical devices [27]. Its other applications include: DSSC counter electrodes [28], sodium-ion battery anode [29], optical material for biological applications [30] and as electrocatalysts [31, 32].

Previously, $FeSe_2$ has been synthesized through diverse techniques *e.g.* solvothermal [27, 31, 32], hydrothermal [28, 29], hot injection [30, 33], selenization [34] and organometallic approach [14]. These methods occurred at elevated temperatures and involved different sources to form the elements (Fe and Se) in iron diselenide. Hence, the methods can be referred to as multiple-source precursors. Some of the drawbacks of these methods include homogeneous pre-reactions, toxic hazards, together with the environmental and safety conditions for the industrial processes [35].

To eliminate the drawbacks of multiple-source precursors, a better approach is to use a complex which contains the targeted elements to be synthesized (*i.e.* the Fe–Se bond). Single-source precursors are compounds in which all the elements to be deposited exist in the complex used for the deposition process. Hence, this results in simplified installations in terms of flow and temperature controls and reduces leak incidence. Also, environmental and safety conditions, being important industrial processes, are taken care of when compared with multiple-source routes. Generally, single-source precursors reduce toxic hazards, eliminate homogeneous pre-reactions, use lower deposition temperatures, afford the intrinsic control of film/nanoparticle stoichiometry, and are cheaper [36, 37, 38].

A major key requirement for single-source precursors is perfection, which eliminates the possible sources of contaminants in the synthesized product, together with unwanted by-products. Other characteristic features of this precursor include: (i) Air and moisture stability. (ii) Less toxicity. (iii) Possibility of low-temperature growth. (iv) impurity incorporation control through ligand design. (v) differences between sources of elements are removed (vi) elimination of heat differences between different complexes used as starting materials (vii) intrinsic control of film stoichiometry. The synthesis of the material through single-source precursor should be possible on an industrial scale without problems such as cost and environmental impact [39].

Pyrolysis (also known as thermolysis or melt reaction) is a solventless reaction which involves subjecting a complex to heat under nitrogen, thereby effecting its breakdown. The solventless methodology of this technique affords both possible cost and health benefits over other techniques that use flammable solvents and complexes. In comparison, pyrolysis is easier and more scalable [40]. This technique makes it possible to understand the connection between precursor structure and nanomaterial shape, thereby controlling it [41, 42]. This solventless method reduces collision between particles, to provide growth through the addition of monomers [41, 42]. Through pyrolysis, diverse semiconductor materials with various morphologies have been synthesised. This might provide a great potential to investigate various precursor chemistry, and understand how the condition(s) of the synthesis and the geometry of complex(es) controls the morphology and contents of the products. Hence, this can be a commercially viable approach for the production of semiconductors [38].

This work explains the preparation of iron (III) thioselenoimidodiphosphinate complex, and investigated its ability to generate $FeSe_2$. This was obtained through a pyrolysis experiment at 500 °C using a glass rod, under reduced pressure for 1 h 30 min. The black product was investigated by XRD, SEM, EDAX and XPS studies. The magnetism exhibited by the deposited $FeSe_2$ was determined by a SQUID magnetometer.

2. Experimental

All reactions occurred under nitrogen by using a Schlenk line, connected to a vacuum pump, and a source of dry nitrogen. All chemicals (from Merck and Fischer) were used unaltered. All solvents were dried and obtained either through distillation or proper storage over molecular sieves. CHN analysis was done at the School of Chemistry, University of Manchester. TGA measurements occurred with Seiko SSC5200/S220TG/DTA at 10 °C/min under an inert atmosphere. Bruker Avance (III) 400 MHz FT-NMR spectrometer was used to determine nuclear magnetic resonance, using deuterated solvents. Proton NMR chemical shifts were reported in reference to tetramethylsilane, while phosphorus NMR chemical shifts were referenced to tetraoxophosphate(V) acid. Mass spectrometry was done with electrospray method at the Mass spectrometry unit, School of Chemistry, University of Manchester, UK.

2.1. Synthesis of [$Ph_2P(S)HNP(Se)Ph_2$] [43]

A solution of chlorodiphenylphosphine (23.88 g, 20 mL, 108.23 mmol) in toluene (25 mL) was added in drops to that of 1,1,1,3,3,3-hexamethydisilazane (8.73 g, 11.42 mL, 54.12 mmol) in toluene for half an hour. This was stirred and heated for 3 h at 90 °C, and the reaction attained an ambient temperature afterwards. Powdered selenium (4.27 g, 54.12 mmol) was added, and the mixture stirred overnight. This was followed by sulphur powder (1.73 g, 54.12 mmol) and also stirred for 7 h. The off-white crude product was recovered from dichloromethane and produced a whitish-yellow powder. Yield: 14.1 g (52%). Micro Analysis: Calcd for $C_{24}H_{21}NP_2SSe$: C, 58.06; H, 4.27; N, 2.82. Found: C, 57.60; H, 4.28; N, 2.93. $^{31}P\text{-}\{^1H\}$ NMR: 52.76, 52.72 ppm; $^1J_{P\text{-}Se} = 496$ Hz. ES + ve MS: m/z 496 corresponds to [$Ph_2P(S)HNP(Se)Ph_2$].

2.2. Synthesis of [$Fe\{(SePPh_2NPPh_2S)_2N\}_3$]

Imidotetraphenylthioselenodiphosphinate ligand (5.00 g, 9.45 mmol) and *tert*-potassium butoxide (^{t}BuOK 1.06 g, 9.45 mmol) was liquified in methanol (50 mL) for an in-situ deprotonation. Solution was stirred under nitrogen at an ambient temperature for 40 min, followed by the dropwise addition of anhydrous $FeCl_3$ as a powder solution (0.51 g, 3.15 mmol). Reaction was stopped after 5 h, and the resulting deep-brown solution mixture was filtered and recrystallized in hot dichloromethane which yielded a brownish-green powder (Scheme 1). Yield: 1.13 g (22%). M. Pt: 217 °C. CHN analysis for $C_{72}H_{60}N_3P_6S_3Se_3Fe$ Calculated: C, 56.1; H, 3.9; N, 2.7; P, 12.1; S, 6.2; Fe, 3.6. Found: C, 55.7; H, 4.1; N, 2.4; P, 11.5; S, 6.9; Fe, 3.2. ^1H NMR (d_8- Toluene): 7.2–6.8 (m, 48H, Ar*H*), 8.3–7.6 (m, 12H, Ar*H*); $^{31}P\{^1H\}$ NMR: 47.38, 30.41 ppm. ES + ve MS: *m/z* 1048 corresponds to [$Fe\{(SePPh_2NPPh_2S)_2N\}_3$].

2.3. Pyrolysis of complex

Thermolysis experiments occurred in a quartz glass rod in a Carbolite furnace. Under a reduced pressure, the complex was heated at 500 °C for 1 h 30 min. Afterwards, the reaction attained an ambient temperature in an inert atmosphere during 60 min. 0.50 g of the complex was pyrolysed for the experiment. The black residue obtained was grinded to powder, followed by different characterisation.

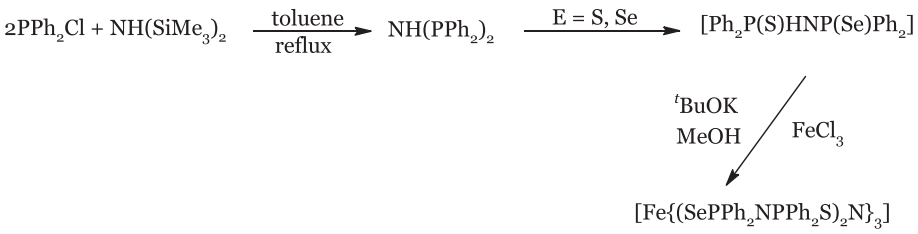

Scheme 1. The reaction scheme for the synthesis of the complex.

2.4. Characterisation of black deposits

XRD was done using a Bruker AXS D8 diffractometer having a monochromated radiation. Samples were scanned between 15 and 85° at 9 s count rate and 0.05 step size. Obtained diffractograms were compared with the ICDD index. Philips XL30 FEG was used for SEM studies, and prior to this, samples were carbon-coated to eliminate charging. EDAX was done with a DX4 instrument. Kratos Axis Ultra spectrometer measured the XPS with an analyser pass energy of 80 and 20 eV for wide and narrow scans respectively. Charges were neutralised consistently on the light-emitting surface with a system base pressure of 5 x 10^{-10} mBar. Spectra analyses occurred through subtraction and peak fitting by Gaussian line shape. Peaks were analysed quantitatively through Scofield elemental sensitivities. Binding energy values were recorded in reference to adventitious contamination peaks at 285 eV, while elemental references were used to adjust the analyser. The magnetic property of the sample was measured between 2 and 300 K, using a SQUID magnetometer. All samples were measured in eicosane to remove the positional effects of high magnetism. Sample holder and eicosane were measured for diamagnetism in advance. FC and ZFC magnetization curves were collected in an applied magnetism of 100 Oe. Isothermal magnetisation curves were recorded between -4 and 4 T magnetic fields at temperatures of 300 K and 5 K.

3. Results and discussion

The geometry of paramagnetic d^5 iron(III) complex summarised in Scheme 1 was possible using elemental analysis. The physical properties of the precursor studied by TGA revealed the breakdown pathway of the complex which occurred in one step, with a quick loss of weight from 303 to 438 °C at 72 %, with a residual mass of 28 % (Fig. S1, supplemental file (SF)).

After pyrolysing the compound at 500 °C, the resulting black powder was pulverized and analyzed by XRD. The pattern indicated by the XRD confirmed that the deposited material was orthorhombic ferroselite $FeSe_2$ (ICDD no. 04-003-1738) mixed with monoclinic Fe_3Se_4 (ICDD no 03-065-2315) (Figure 1). Traces of Fe_3Se_4 were also evident at 2θ values of 29.09 and 31.77°. The obtained values for the lattice parameters: a = 4.8019 (9) Å, b = 5.786(3) Å and c = 3.5844 (4) Å are consistent with those in the literature [44, 45]. For the monoclinic Fe_3Se_4, the obtained lattice parameters were: a = 6.2024 (3) Å, b = 3.5320 (2) Å and c = 11.2800 (6) Å, which are all quite close to the reported values [46]. However, when the deposition temperature was increased to 550 °C, a different pattern was obtained which could not be matched to any phase of iron selenide. Hence, this pattern did not correspond to any material (Figure 2). The reason(s) for this is/are unclear.

Previously, orthorhombic ferroselite $FeSe_2$ was deposited from a solution-based decomposition in oleylamine [19], while Fe_3Se_4 was also produced from catalyst-aided CVD experiments [16].

For the $FeSe_2$ deposited from $[Fe\{(SePPh_2)_2N\}_2]$, no XRD measurement was reported for this material, due to the poor quality of the films [12].

The morphology of the synthesised material at 500 °C revealed an irregular polygonal crystallites according to the SEM. However, although the obtained XRD pattern at 550 °C could not be matched to any phase of iron selenide, a similar morphology was also observed for the structure of the material at this temperature (Figure 3 (a&b)).

The EDAX analysis for the pyrolysed sample at 500 °C indicated that the ratio of iron to selenium was close to 1:2 with 10% sulphur. The sample obtained at 550 °C has a higher content of iron, and the iron to selenium ratio was also close to 1:2 with 12% sulphur content.

The XPS measurements of the deposited $FeSe_2$ indicated the binding energy of Fe $2p_{3/2}$ peak at 713 eV, and Fe $2p_{1/2}$ peak occurred at 728 eV, which corresponds to iron oxide (Figure 4a). This indicated the easy oxidation of the prepared $FeSe_2$ in air, which revealed its surface oxidation before XPS measurements. This showed that the surface of the deposited powders was contaminated with oxygen. Hence, iron at the surface and near surface region of the powder seemed to be attached to

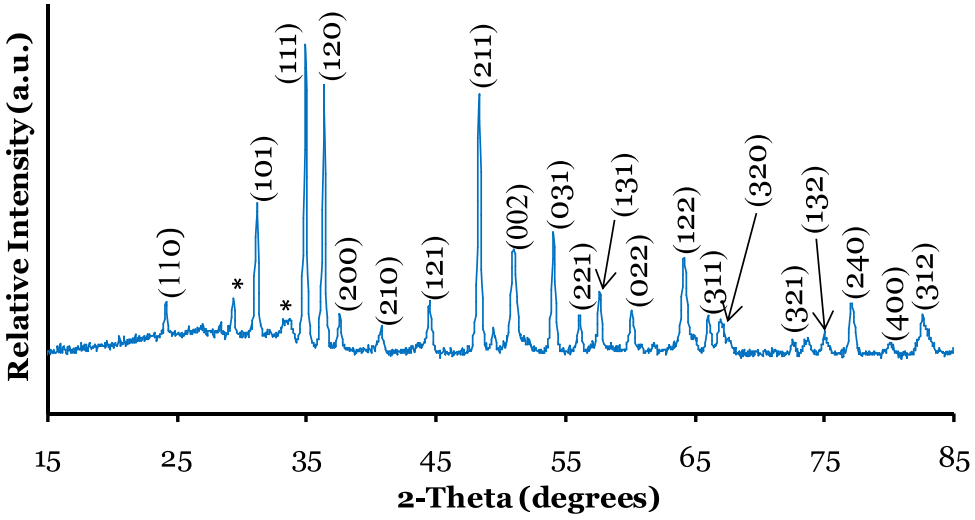

Figure 1. X-Ray diffractogram of orthorhombic $FeSe_2$ prepared at 500 °C. Marked peaks correspond to Fe_3Se_4.

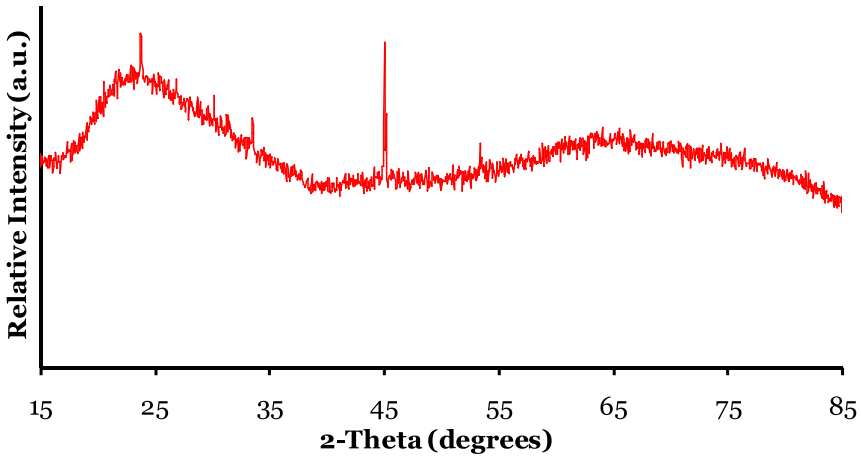

Figure 2. The unmatched XRD pattern obtained from pyrolysis of the complex at 550 °C.

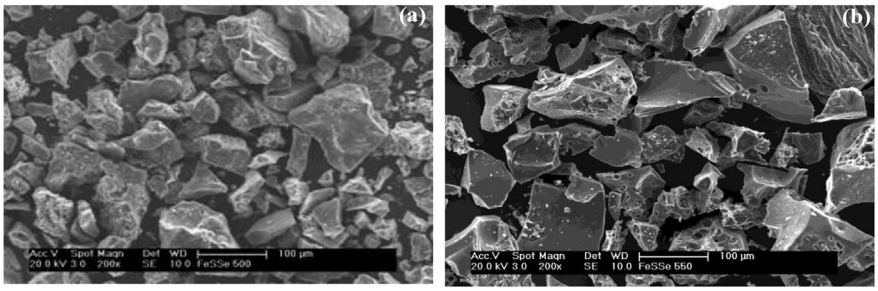

Figure 3. Pictorial representation for orthorhombic $FeSe_2$ prepared at: (a) 500 °C, (b) unmatched pattern at 550 °C as shown by the SEM.

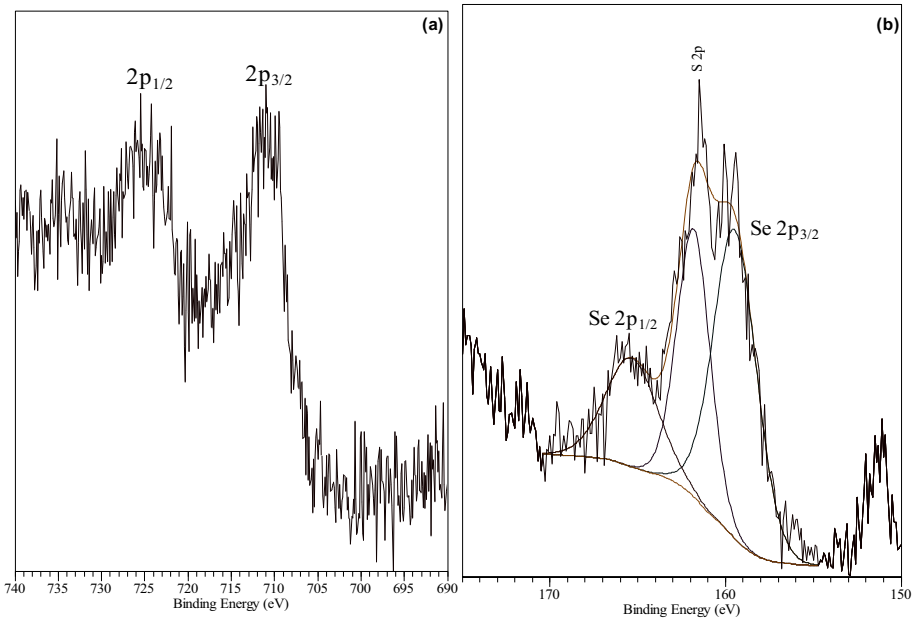

Figure 4. X-ray photoelectron spectroscopy of: (a) Fe 2p, (b) Se 2p peaks.

oxygen. The Se $2p_{3/2}$ peak at 159.5 eV is more consistent with a selenide oxide species (Figure 4b). The S and Se peaks were identified by the overlapping S and Se 2p features near 160 eV as the Se 2s was covered by the S 2s peak. It might be explained that prior oxidation had occurred during other characterisations. Previous reports on $FeSe_2$ nanorods [14] and thin film [47] also observed similar surface oxidation of the material.

The deposited powder from the pyrolysis of [Fe $\{(SePPh_2NPPh_2S)_2N\}_3$] complex revealed temperature-dependent hysteresis. This is expected because of the presence of crystallographic $FeSe_2$ which exhibits hysteretic features. $FeSe_2$ powder exhibited hysteretic features at 5, 30 and 300 K (Figure 5a), since the magnetization curve depends on the field. Anisotropic energy determines the magnetization of

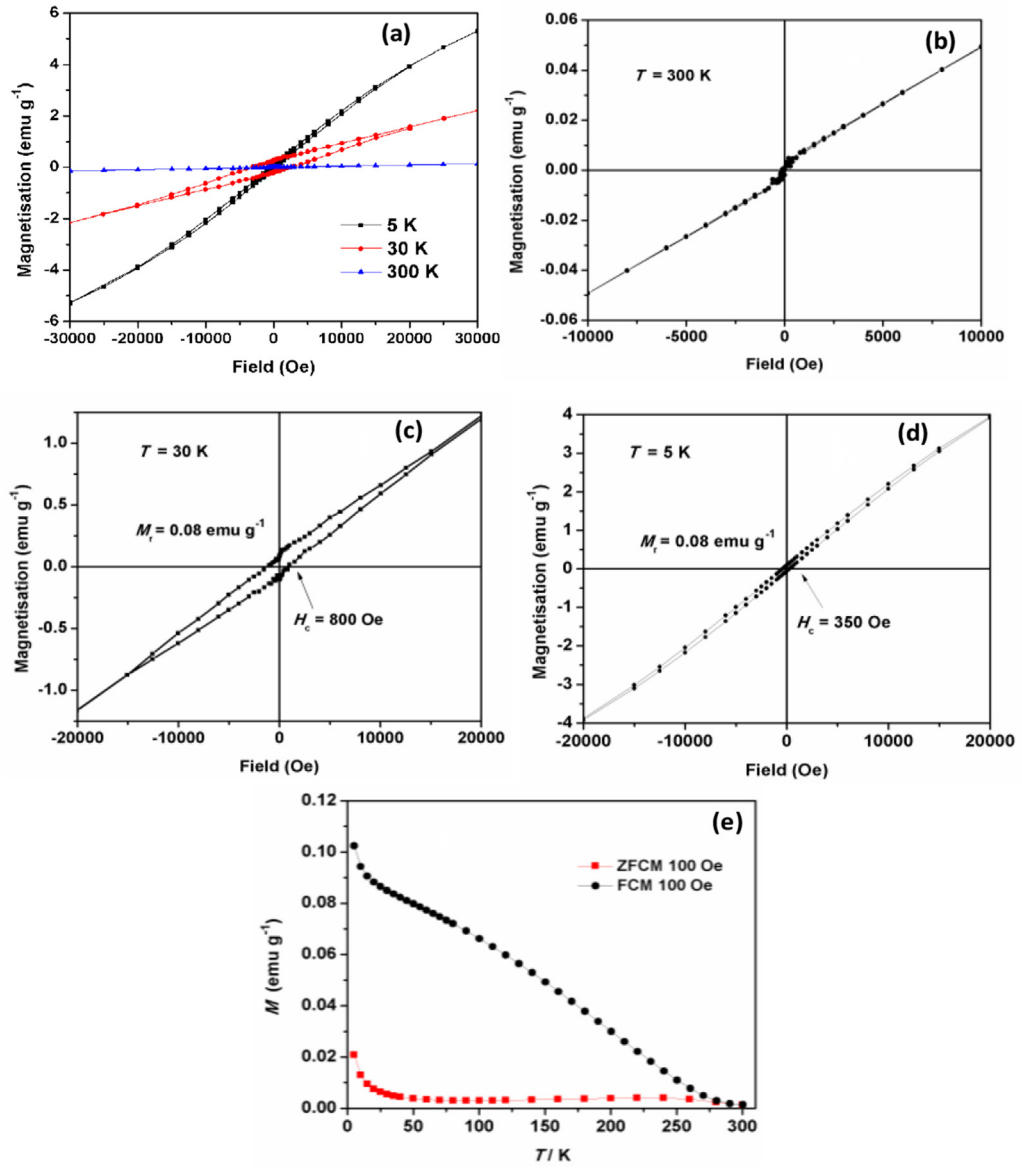

Figure 5. (a) Magnetic hysteresis at 5, 30 and 300 K for iron selenide powder. (b) Hysteresis loop at 300 K for iron selenide powder. (c) Magnetic hysteresis at 30 K for iron selenide powder. (d) Hysteresis loop at 5 K for iron selenide powder. (e) Temperature dependence of the ZFC and FC magnetisation curve for $FeSe_2$ in an applied magnetic field of 100 Oe.

any magnetic material, and this energy restricts the magnetism alignment in a definite axis called the easy axis. For a nanoparticle, the highest value of anisotropic energy depends on the combined effects of its volume (V), and constant (K) [48]. In a magnetic system, the blocking temperature, T_B, is that above which the thermal energy is sufficient for the free alignment of magnetization in arbitrary directions [49]. The magnetism graphs of FC and ZFC can be used to deduce the blocking temperature (T_B). Graphically, this occurs when the slope of zero field cooled curve tends towards zero. At 300 K, the deposited $FeSe_2$ is in its super paramagnetic state, with negligible remanence and coercivity (Figure 5b). At the lower temperatures, $FeSe_2$ exhibited hysteretic behaviour, and the effect is more pronounced at 30 K (Figures 5c and 5d). The coercive field and remanant magnetization values are listed on each graph.

At Curie temperature above 300 K, $FeSe_2$ exhibits permanent magnetic effect [50, 51]. There were no magnetic measurements reported for iron selenide synthesised from $[Fe\{(SePPh_2)_2N\}_2]$ [12]. From the deposited iron selenide powder in this work, the field cooled and zero-field cooled magnetization curves were obtained. The divergence of the ZFC and FC with decreasing temperature indicated the existence of a sequential arrangement of magnetism (hence the ferromagnetism), probably due to the immense changes in the magnetic property (Figure 4e). A transition temperature around 280 K was observed for the iron selenide powder. As typical of ferromagnetic materials, the hysteresis loops obtained from the deposited iron selenide exhibited a linear decrease in the room temperature magnetization with an increase in the magnetic field. This might be because of the minimal inconsistencies in the temperature of the magnetism.

4. Conclusions

Thioselenoimidodiphosphinate complex of iron, $[Fe\{(SePPh_2NPPh_2S)_2N\}_3]$ was synthesised through a metathetical reaction and its ability to generate iron selenide was studied. Pictorial images for the morphology of the $FeSe_2$ powder revealed polygons of orthorhombic ferroselite $FeSe_2$ according to the SEM. Magnetic studies on $FeSe_2$ revealed its ferromagnetism, having changes in its properties at a temperature around 280 K. Using complexes that contain the targeted elements to be synthesised, pyrolysis affords the opportunity to control

reaction conditions, which determines the size, shape and chemistry of the targeted materials. The precursors in pyrolysis are easier to handle, and the process of heating them in a furnace should be cheaper and easier to scale up. Although the major barrier of pyrolysis seems that it is largely unexplored, however, this might be a potentially economically viable route to produce orthorhombic $FeSe_2$ with desired/targeted properties. Future work on this complex will focus on the synthesis of the more volatile isopropyl analogue, together with AACVD studies of its capability to deposit mixed phases of iron chalcogenide.

Declarations

Author contribution statement

Martins O. Omorogie: Analyzed and interpreted the data; Wrote the paper.

Temidayo Oyetunde: Conceived and designed the experiments; Performed the experiments; Analyzed and interpreted the data; Wrote the paper.

Paul O'Brien: Conceived and designed the experiments; Analyzed and interpreted the data; Contributed reagents, materials, analysis tools or data.

Funding statement

This research did not receive any specific grant from funding agencies in the public, commercial, or not-for-profit sectors.

Competing interest statement

The authors declare no conflict of interest.

Additional information

Supplementary content related to this article has been published online at https://doi.org/10.1016/j.heliyon.2020.e03763.

Acknowledgements

The authors are grateful for the contributions from Dr. Paul Wincott (XPS) and Dr. Floriana Tuna (SQUID) on the respective measurements.

References

[1] D. Jasion, J.M. Barforoush, Q. Qiao, Y. Zhu, S. Ren, K.C. Leonard, Low-dimensional hyperthin FeS2 nanostructures for efficient and stable hydrogen evolution electrocatalysis, ACS Catal. 5 (2015) 6653–6657.

[2] H.A. Macpherson, C.R. Stoldt, Iron pyrite nanocubes: size and shape considerations for photovoltaic application, ACS Nano 6 (2012) 8940–8949.

[3] J.-W. Choi, G. Cheruvally, H.-J. Ahn, K.-W. Kim, J.-H. Ahn, Electrochemical characteristics of room temperature Li/FeS2 batteries with natural pyrite cathode, J. Power Sources 163 (2006) 158–165.

[4] Z. Yin, K. Haule, G. Kotliar, Kinetic frustration and the nature of the magnetic and paramagnetic states in iron pnictides and iron chalcogenides, Nat. Mater. 10 (2011) 932.

[5] M.-R. Gao, Y.-F. Xu, J. Jiang, S.-H. Yu, Nanostructured metal chalcogenides: synthesis, modification, and applications in energy conversion and storage devices, Chem. Soc. Rev. 42 (2013) 2986–3017.

[6] Y.-X. Wang, J. Yang, S.-L. Chou, H.K. Liu, W.-x. Zhang, D. Zhao, S.X. Dou, Uniform yolk-shell iron sulfide–carbon nanospheres for superior sodium–iron sulfide batteries, Nat. Commun. 6 (2015) 8689.

[7] M. Barawi, I.J. Ferrer, E. Flores, S. Yoda, J.R. Ares, C. Sánchez, Hydrogen photoassisted generation by visible light and an earth abundant photocatalyst: pyrite (FeS2), J. Phys. Chem. C 120 (2016) 9547–9552.

[8] P.D. Matthews, M. Akhtar, M.A. Malik, N. Revaprasadu, P. O'Brien, Synthetic routes to iron chalcogenide nanoparticles and thin films, Dalton Trans. 45 (2016) 18803–18812.

[9] M. Akhtar, A.L. Abdelhady, M.A. Malik, P. O'Brien, Deposition of iron sulfide thin films by AACVD from single source precursors, J. Cryst. Growth 346 (2012) 106–112.

[10] M. Akhtar, J. Akhtar, M.A. Malik, F. Tuna, M. Helliwell, P. O'Brien, Deposition of iron selenide nanocrystals and thin films from tris (N, N-diethyl-N′-naphthoylselenoureato) iron (iii), J. Mater. Chem. 22 (2012) 14970–14975.

[11] M. Akhtar, J. Akhter, M.A. Malik, P. O'Brien, F. Tuna, J. Raftery, M. Helliwell, Deposition of iron sulfide nanocrystals from single source precursors, J. Mater. Chem. 21 (2011) 9737–9745.

[12] M. Akhtar, M.A. Malik, J. Raftery, P. O'Brien, Synthesis of iron selenide nanocrystals and thin films from bis (tetraisopropyldiselenoimidodiphosphinato) iron (II) and bis (tetraphenyldiselenoimidodiphosphinato) iron (II) complexes, J. Mater. Chem. 2 (2014) 20612–20620.

[13] M. Akhtar, M.A. Malik, F. Tuna, P. O'Brien, The synthesis of iron sulfide nanocrystals from tris (O-alkylxanthato) iron (III) complexes, J. Mater. Chem. 1 (2013) 8766–8774.

[14] J. Xu, K. Jang, J. Lee, H.J. Kim, J. Jeong, J.-G. Park, S.U. Son, Phase-selective growth of assembled FeSe2 nanorods from organometallic polymers and their surface magnetism, Cryst. Growth Des. 11 (2011) 2707–2710.

[15] H.J. Kwon, S. Thanikaikarasan, T. Mahalingam, K.H. Park, C. Sanjeeviraja, Y.D. Kim, Characterization of electrosynthesized iron diselenide thin films, J. Mater. Sci. Mater. Electron. 19 (2008) 1086–1091.

[16] T. Mahalingam, S. Thanikaikarasan, R. Chandramohan, M. Raja, C. Sanjeeviraja, J.-H. Kim, Y.D. Kim, Effects of bath temperature in electrodeposited FeSe2 thin films, Mater. Chem. Phys. 106 (2007) 369–374.

[17] G. Li, B. Zhang, J. Rao, D. Herranz Gonzalez, G.R. Blake, R.A. de Groot, T.T. Palstra, Effect of vacancies on magnetism, electrical transport, and thermoelectric performance of marcasite FeSe2− δ (δ= 0.05), Chem. Mater. 27 (2015) 8220–8229.

[18] K.D. Oyler, X. Ke, I.T. Sines, P. Schiffer, R.E. Schaak, Chemical synthesis of two-dimensional iron chalcogenide nanosheets: FeSe, FeTe, Fe (Se, Te), and FeTe2, Chem. Mater. 21 (2009) 3655–3661.

[19] L. Wu, J. Zhang, C. Wang, J. Li, Influence of compositional ratio K/Na on physical properties in (K x Na 1−x) NbO 3 ceramics, J. Appl. Phys. 103 (2008), 084116.

[20] R.A. Hussain, A. Badshah, A. Younis, M.D. Khan, J. Akhtar, Iron selenide films by aerosol assisted chemical vapor deposition from single source organometallic precursor in the presence of surfactants, Thin Solid Films 567 (2014) 58–63.

[21] N. Levesanos, W.P. Liyanage, E. Ferentinos, G. Raptopoulos, P. Paraskevopoulou, Y. Sanakis, A. Choudhury, P. Stavropoulos, M. Nath, P. Kyritsis, Investigating the structural, spectroscopic, and electrochemical properties of [Fe {(EPiPr2) 2N} 2](E= S, Se) and the formation of iron selenides by chemical vapor deposition, Eur. J. Inorg. Chem. 2016 (2016) 5332–5339.

[22] S. Thanikaikarasan, T. Mahalingam, K. Sundaram, A. Kathalingam, Y.D. Kim, T. Kim, Growth and characterization of electrosynthesized iron selenide thin films, Vacuum 83 (2009) 1066–1072.

[23] Y. Han, W. Li, L. Cao, S. Zhang, B. Xu, B. Zhao, Preparation and superconductivity of iron selenide thin films, J. Phys. Condens. Matter 21 (2009) 235702.

[24] H. Zhang, G. Long, D. Li, R. Sabirianov, H. Zeng, Fe3Se4 nanostructures with giant coercivity synthesized by solution chemistry, Chem. Mater. 23 (2011) 3769–3774.

[25] L. Chen, H. Zhan, X. Yang, Z. Sun, J. Zhang, D. Xu, C. Liang, M. Wu, J. Fang, Composition and size tailored synthesis of iron selenide nanoflakes, CrystEngComm 12 (2010) 4386–4391.

[26] B. Yuan, X. Hou, Y. Han, W. Luan, S.-t. Tu, Facile synthesis of flake-like FeSe 2 particles in open-air conditions, New J. Chem. 36 (2012) 2101–2105.

[27] C. Wei, Y. Bai, A. Deng, Y. Bao, Universal synthesis of air stable, phase pure, controllable FeSe2 nanocrystals, Nanotechnology 27 (2016) 165702.

[28] W. Wang, X. Pan, W. Liu, B. Zhang, H. Chen, X. Fang, J. Yao, S. Dai, FeSe 2 films with controllable morphologies as efficient counter electrodes for dye-sensitized solar cells, Chem. Commun. 50 (2014) 2618–2620.

[29] K. Zhang, Z. Hu, X. Liu, Z. Tao, J. Chen, FeSe2 microspheres as a high-performance anode material for Na-ion batteries, Adv. Mater. 27 (2015) 3305–3309.

[30] X. Mao, J.-G. Kim, J. Han, H.S. Jung, S.G. Lee, N.A. Kotov, J. Lee, Phase-pure FeSe x (x= 1, 2) nanoparticles with one-and two-photon luminescence, J. Am. Chem. Soc. 136 (2014) 7189–7192.

[31] X. Xu, Y. Ge, M. Wang, Z. Zhang, P. Dong, R. Baines, M. Ye, J. Shen, Cobalt-doped FeSe2-RGO as highly active and stable electrocatalysts for hydrogen evolution reactions, ACS Appl. Mater. Interfaces 8 (2016) 18036–18042.

[32] R. Shwetharani, D. Nagaraju, R.G. Balakrishna, V. Suvina, Hydrogenase enzyme like nanocatalysts FeS2 and FeSe2 for molecular hydrogen evolution reaction, Mater. Lett. 248 (2019) 39–42.

[33] D. Deng, C. Hao, S. Sen, C. Xu, P. Král, N.A. Kotov, Template-free hierarchical self-assembly of iron diselenide nanoparticles into mesoscale hedgehogs, J. Am. Chem. Soc. 139 (2017) 16630–16639.

[34] B. Ouertani, J. Ouerfelli, M. Saadoun, M. Zribi, M.B. Rabha, B. Bessais, H. Ezzaouia, Optical and structural properties of FeSe2 thin films obtained by selenization of sprayed amorphous iron oxide films, Thin Solid Films 511 (2006) 457–462.

[35] A.N. Gleizes, MOCVD of chalcogenides, pnictides, and heterometallic compounds from single-source molecule precursors, Chem. Vap. Depos. 6 (2000) 155–173.

[36] M.A. Malik, M. Afzaal, P. O'Brien, Precursor chemistry for main group elements in semiconducting materials, Chem. Rev. 110 (2010) 4417–4446.

[37] A.C. Jones, P. O'Brien, CVD of Compound Semiconductors: Precursor Synthesis, Development and Applications, VCH, Weinheim, 1997, 1997.

[38] E. Lewis, S. Haigh, P. O'Brien, The synthesis of metallic and semiconducting nanoparticles from reactive melts of precursors, J. Mater. Chem. 2 (2014) 570–580.

[39] J. Chen, L.-M. Wu, L. Chen, Syntheses and characterizations of bismuth nanofilms and nanorhombuses by the structure-controlling solventless method, Inorg. Chem. 46 (2007) 586–591.

[40] L. Chen, L.-M. Wu, Solventless thermolysis: a possible bridge between crystal structure and nanosynthesis? Inorg. Chem. Focus III (2006) 295.

[41] T.H. Larsen, M. Sigman, A. Ghezelbash, R.C. Doty, B.A. Korgel, Solventless synthesis of copper sulfide nanorods by thermolysis of a single source thiolate-derived precursor, J. Am. Chem. Soc. 125 (2003) 5638–5639.
[42] L. Chen, Y.-B. Chen, L.-M. Wu, Synthesis of uniform Cu2S nanowires from Copper–thiolate polymer precursors by a solventless thermolytic method, J. Am. Chem. Soc. 126 (2004) 16334–16335.
[43] D. Cupertino, D.J. Birdsall, A.M. Slawin, J.D. Woollins, The preparation and coordination chemistry of iPr2P (E) NHP (E′) iPr2 (E, E′= Se; E= Se, E′= S; E= S, E′= O; E, E′= O, Inorg. Chim. Acta. 290 (1999) 1–7.
[44] B. Lavina, R. Downs, S. Sinogeikin, The structure of ferroselite, FeSe2, at pressures up to 46 GPa and temperatures down to 50 K: A single-crystal micro-diffraction analysis, Crystals 8 (2018) 289.
[45] J.D. Woollins, P–N–S/Se-containing metallacycles, J. Chem. Soc., Dalton Trans. (1996) 2893–2901.
[46] R. Pohjonen, O. Mustonen, M. Karppinen, J. Lindén, Mössbauer study of magnetism in Fe3Se4, J. Alloys Compd. 746 (2018) 135–139.
[47] N. Hamdadou, A. Khelil, M. Morsli, J. Bernade, Iron diselenide thin films synthesized by soft selenization of iron films, Vacuum 77 (2005) 151–156.
[48] G.F. Goya, T. Berquo, F. Fonseca, M. Morales, Static and dynamic magnetic properties of spherical magnetite nanoparticles, J. Appl. Phys. 94 (2003) 3520–3528.
[49] V.S. Coker, N.D. Telling, G. van der Laan, R.A. Pattrick, C.I. Pearce, E. Arenholz, F. Tuna, R.E. Winpenny, J.R. Lloyd, Harnessing the extracellular bacterial production of nanoscale cobalt ferrite with exploitable magnetic properties, ACS Nano 3 (2009) 1922–1928.
[50] M.R. Gao, Z.Y. Lin, J. Jiang, H.B. Yao, Y.M. Lu, Q. Gao, W.T. Yao, S.H. Yu, Selective synthesis of Fe7Se8 polyhedra with exposed high-index facets and Fe7Se8 nanorods by a solvothermal process in a binary solution and their collective intrinsic properties, Chem. Eur J. 17 (2011) 5068–5075.
[51] Q. Feng, D. Shen, J. Zhang, B. Li, B. Li, Y. Lu, X. Fan, H. Liang, Ferromagnetic FeSe: structural, electrical, and magnetic properties, Appl. Phys. Lett. 88 (2006), 012505.